Journal of Catalysis 266 (2009) 156–163

Contents lists available at ScienceDirect

Journal of Catalysis

journal homepage: www.elsevier.com/locate/jcat

Surface and structure characteristics of carbon-supported Pd_3Pt_1 bimetallic nanoparticles for methanol-tolerant oxygen reduction reaction

Wenming Wang [a,b], Qinghong Huang [a], Juanying Liu [a], Zhiqing Zou [a], Miaoying Zhao [a], Walter Vogel [c], Hui Yang [a,*]

[a] Energy Science and Technology Laboratory, Shanghai Institute of Microsystem and Information Technology, Chinese Academy of Sciences, Shanghai 200050, China
[b] Department of Electric Power, Hunan Electric Power Design Institute, Hunan 410007, China
[c] Department of Chemistry, National Central University, Taoyuan, Taiwan 32001, China

ARTICLE INFO

Article history:
Received 9 April 2009
Revised 26 May 2009
Accepted 4 June 2009
Available online 2 July 2009

Keywords:
Surface and structure-controlled synthesis
Pd_3Pt_1 bimetallic nanoparticle
Oxygen reduction reaction
Electrocatalysis
Methanol tolerance
In situ X-ray diffraction

ABSTRACT

Surface and structure of carbon-supported Pd_3Pt_1 (Pd_3Pt_1/C) bimetallic nanoparticles of small particle size can be tuned during synthesis through the use or nonuse of trisodium citrate (TC) as the complexing agent. The addition of TC during the synthesis results in Pd enrichment on the surface layers of the Pd_3Pt_1/C catalysts and to an abnormal lattice expansion as compared to that of pure Pd/C and Pt/C. However, without the addition of TC, a normal lattice constant and Pt enrichment on the surface layers of the catalysts are obtained. Among the prepared catalysts, the maximum activity for the oxygen reduction reaction (ORR) occurs for Pd_3Pt_1/C catalyst with Pt surface enrichment. Importantly, the Pd_3Pt_1/C catalysts with Pd surface enrichment exhibited substantially higher methanol tolerance during the ORR than both the Pd_3Pt_1/C catalyst with Pt surface enrichment and the Pt/C catalyst. Thus, Pd_3Pt_1/C catalysts may represent a methanol-tolerant ORR cathode catalyst.

1. Introduction

Recently, direct methanol fuel cells (DMFCs) have attracted a considerable attention due to their potential applications in portable devices [1,2]. However, methanol crossover from the anode to the cathode is a major hurdle that DMFCs must surmount in order to reach their commercialization. This problem derives from the fact that the commonly used expensive Pt-based cathode catalysts are also active for the adsorption and oxidation of methanol [3], and intrinsic methanol crossover from the anode to the cathode results not only in a mixed potential effect at the cathode, but also decreases fuel utilization. Efforts to avoid these detrimental prospects have involved the development of novel and less methanol permeable membranes [4,5] and the utilization of new oxygen reduction catalysts that exhibit high oxygen reduction reaction activity and high methanol tolerance [6–22].

Thus, considering the cost of Pt cathode material that is normally used, the issue of methanol tolerance and stability is imperative that new electrocatalysts be developed for the oxygen reduction reaction (ORR). Considerable attention has, in fact, focused on the development of Pd-based alloy nanoparticles, not only because of lower costs and greater abundance, but also especially because of the lower reactivity of Pd-based alloys to the adsorption and oxidation of methanol, which is of great importance for the improved methanol tolerance in a DMFC [3,9–22].

Numerous studies over the past few years have shown that the catalytic activity of Pd for the ORR could be improved significantly by adding non-noble metal (M) elements, such as Co, Fe, and Ni [3,9–22]. The enhancement in ORR activity has been attributed to several factors, including effects that are electronic and structural in nature. However, these non-noble metal elements might have a strong potential to leach out under electrochemical conditions, as indicated in the prior investigations for Pt–M catalysts [23–25]. Under DMFC operating conditions, the dissolution of the non-noble metal components within the Pd alloys might lead to limited lifetime of the DMFC. To avoid this potential problem, studies have involved the utilization of PdPt-based electrocatalysts for the ORR and methanol-tolerant ORR, because the long-term stability of Pd in acidic solution is comparable with that of Pt [26–29]. It is thus of great importance to investigate the PdPt-based nanosized catalysts as potential methanol-tolerant catalysts for oxygen electroreduction.

It is widely accepted that the electrocatalytic activity of Pt- or Pd-based binary or ternary catalysts is strongly influenced by bulk and/or surface composition, the microscopic nature of the structure, the local arrangement of atoms in the metallic core of the nanoparticles, and the dispersion of nanoparticles [30]. However,

* Corresponding author. Fax: +86 21 32200534.
E-mail addresses: hyang@mail.sim.ac.cn, huiyang65@hotmail.com (H. Yang).

0021-9517/$ - see front matter © 2009 Elsevier Inc. All rights reserved.
doi:10.1016/j.jcat.2009.06.004

synthesis procedures that result in catalysts with desirable bulk and/or surface composition, suitable microstructure and controlled nanoparticle size with a narrow dispersion have remained an enormous challenge.

Here, we report a novel strategy for surface and structure-controlled synthesis of carbon-supported Pd_3Pt_1 nanoparticles (Pd_3Pt_1/C) for the ORR as well as for methanol-tolerant ORR. The as-prepared Pd_3Pt_1 catalysts have been characterized by various physical and electrochemical techniques, including X-ray diffraction at wide angles (WAXS), with line profile fitting using Pearson-VII type functions to evaluate the structure of the bimetallic catalysts, and electrocatalytic activities of the nanoparticle catalysts for the ORR. The possible influence of surface composition and structure of the Pd_3Pt_1/C on the ORR activity in the absence and presence of methanol is also reported.

2. Experimental

2.1. Catalyst synthesis

The Pd_3Pt_1/C catalysts with Pt enrichment on the surface layers of the catalysts were synthesized via a facile, one-step synthesis route. Ethylene glycol (EG) was used as solvent and reducing agent. In brief, 80.0 mg of XC-72R carbon, 35.7 mg of palladium acetylacetonate [$Pd(acac)_2$], and 15.8 mg of platinum acetylacetonate [$Pt(acac)_2$] were dissolved in 50 mL of EG to form a mixture. Such a reacting mixture was then maintained at an optimized refluxing temperature of 175 °C in a three-necked flask for 6 h. After cooling to room temperature, the mixture was filtered, washed, and dried under vacuum at ca. 75 °C for 12 h. The obtained catalyst is denoted as Pd_3Pt_1/C-1. Alternatively, different amounts of TC as a complexing agent and stabilizer [31,32] were added into the above-mentioned reacting mixture before refluxing. Three bimetallic Pd_3Pt_1/C nanoparticle catalysts with Pd enrichment in their surface layers can be synthesized by way of an improved one-step synthesis route. The amounts of TC used were 0.1, 0.15, and 0.2 g in 50 mL of EG, corresponding to a TC/(Pd + Pt) molar ratio of 2.19, 3.28, and 4.38, respectively; resultant catalysts are denoted as Pd_3Pt_1/C-2, Pd_3Pt_1/C-3 and Pd_3Pt_1/C-4, respectively. For the sake of comparison, the Pd/C catalyst was also synthesized with the same procedure. The total metal loading was controlled at 20 wt.% for all the catalysts.

2.2. Physical characterization

The bulk composition analysis of the catalysts was performed with an IRIS Advantage ICP-AES system (Thermo, America). The particle size and morphology of the catalysts were analyzed by transmission electron microscopy (TEM) using a JEOL JEM 2100F instrument operated at 200 kV.

The evaluation of the electronic structure and surface composition of the catalysts was carried out by X-ray photoelectron spectroscopy (XPS) using Al Kα radiation (Kratos AXIS UltraDLD, Britain). The binding energy of the XPS was referenced to the C 1s spectrum of carbon support at 284.45 eV.

X-ray diffraction measurements were carried out on a Guinier powder diffractometer (Huber), set at a 45° transmission angle using the Cu $K\alpha_1$ radiation (λ = 0.15406 nm). The sample containing ca. 10–20 mg of catalyst was slightly pressed to a thin pellet of 0.3 mm thickness. This pellet was then fixed between two 3-μm polyethylene foils into the sample holder. The WAXS patterns were obtained with high resolution in the step-scanning mode with a narrow receiving slit of 0.125 mm, corresponding to 0.125/4° theta. Scans were recorded in the theta-range of 5° to 48° at room temperature. The background-corrected patterns were subjected to the usual angular correction for absorption, polarization, and geometric factors, and plotted versus the reciprocal scattering length $b = 2\sin\theta/\lambda$, where θ is the Bragg angle and λ is the wavelength of the X-ray radiation. The line profile fitting was conducted using five Pearson-VII type functions to extract the integral line width and line positions.

2.3. Electrochemical characterization

Porous electrodes were prepared as described previously [6]. In brief, 10 mg of Pd_3Pt_1/C catalyst, 0.5 mL of Nafion solution (5 wt.%, Aldrich), and 2.5 mL of ultrapure water were mixed ultrasonically. A measured volume (3 μL) of this ink was transferred via a syringe onto a freshly polished glass carbon disk (3 mm diameter). After the solvent was evaporated overnight at room temperature, the electrode was used as the working electrode. Each electrode contained ca. 28 μg cm^{-2} of the metal.

All chemicals used were of analytical grade and all solutions were prepared with ultrapure water (Milli-Q, Millipore). Electrochemical measurements were performed using a CHI 730 Potentiostat and a conventional three-electrode cell. The catalytic activity for the ORR was measured with a RDE (Radiometer, France). The counter electrode was a glass carbon plate, and a saturated calomel electrode was used as the reference electrode. However, electrode potentials in this work are referenced with respect to the reversible hydrogen electrode (RHE). The electrolyte used was 0.1 M $HClO_4$ or 0.1 M $HClO_4$ + 0.5 M CH_3OH. Prior to any electrochemical measurement, the porous electrodes were cycled between 0.05 and 1.00 V/RHE at a scan rate of 50 mV s^{-1} under N_2 until a reproducible cyclic voltammogram (CV) was obtained (ca. 15 cycles). The latter step was conducted to remove contaminants from the electrode; the upper potential was set to ca. 1.00 V/RHE, so that any change in particle size could be avoided. After 15 cycles (until 100 cycles), the CV curves almost kept the same, revealing that the catalysts are stable and that no obvious change in the Pd/Pt surface composition occurs under these conditions. To probe the surface of the catalysts, CO-stripping voltammetric tests were performed as follows: CO was pre-adsorbed onto the catalyst at a given potential of 0.05 V/RHE for 30 min by bubbling CO into 0.1 M $HClO_4$ solution. CO in the solution was subsequently removed by purging with high-purity N_2 for 45 min. High-purity nitrogen or oxygen was used for deaeration of the solutions. During measurements, a gentle gas flow was kept above the electrolyte solution.

All experiments were carried out at a temperature of 25 ± 1 °C.

3. Results and discussion

3.1. The morphology and surface of the Pd_3Pt_1/C bimetallic catalysts

The average bulk composition of the Pd_3Pt_1/C bimetallic catalysts was evaluated using ICP-AES analysis. The results obtained are nearly the same as original stoichiometric values, suggesting that as a result of our synthesis methodology Pd and Pt are totally reduced to form Pd/Pt bimetallic nanoparticles.

Fig. 1 shows TEM images of as-prepared Pd_3Pt_1/C catalysts and their corresponding particle size histograms based on the observation of more than 500 nanoparticles. The obtained mean particle size in diameter and the standard deviation for all the Pd_3Pt_1/C catalysts are given in the figure. The Pd_3Pt_1 bimetallic nanoparticles appear to be well dispersed on the surface of carbon and have a relatively narrow particle size distribution. With increase in TC added during the synthesis, a slight decrease in mean particle size is found, which might be due to the formation of complexes between TC with Pd and Pt (data not shown in this work) and attributable to the co-reduction of Pd and Pt. The synthesis approach used here

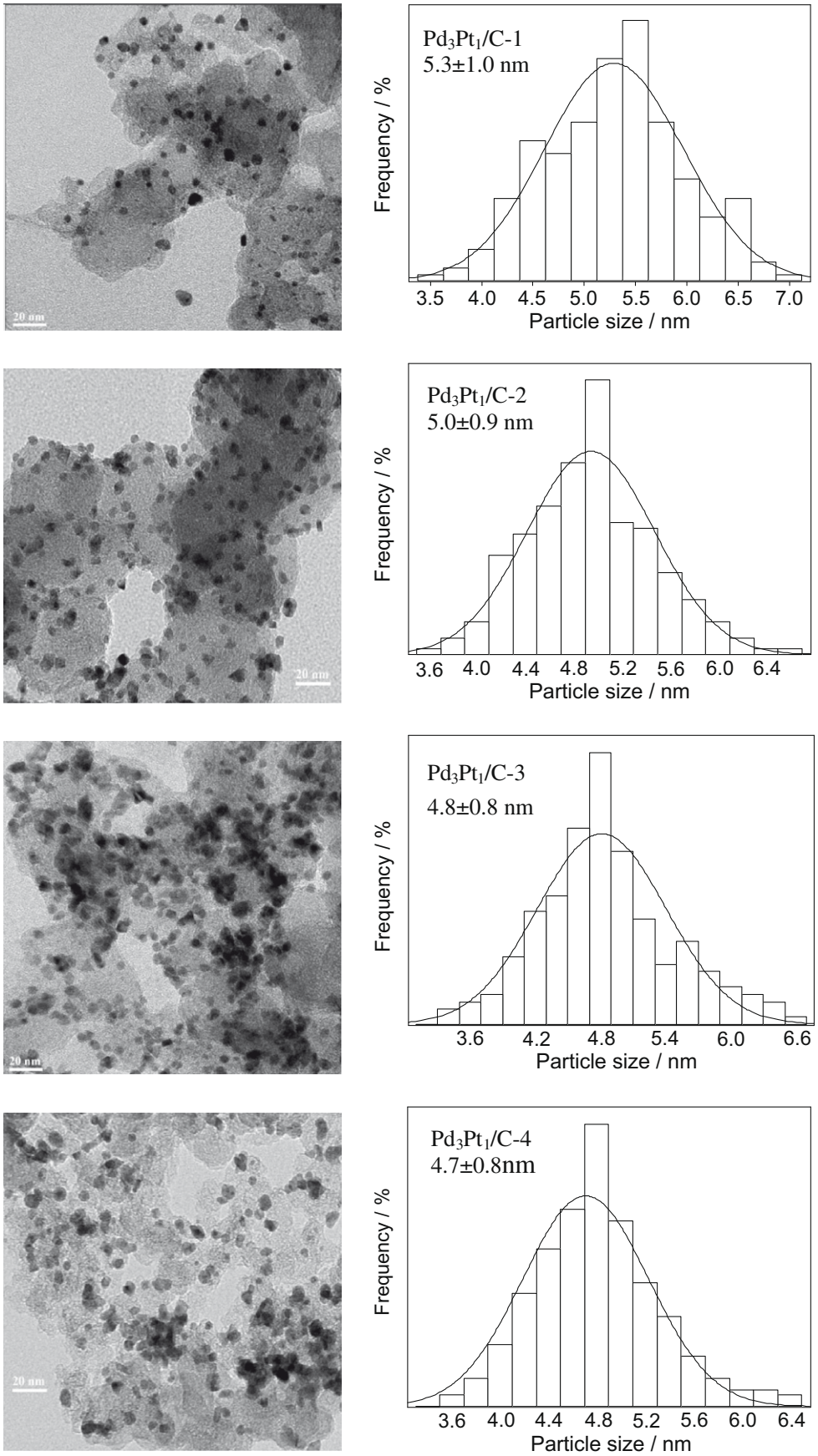

Fig. 1. TEM images of the as-prepared Pd_3Pt_1/C catalysts and their corresponding particle size distribution histograms.

appears to represent an efficient method for obtaining nanostructured bimetallic catalysts with a narrow particle distribution and a good dispersion on the support.

To explore the electronic properties and surface composition of the Pd_3Pt_1/C catalysts, two typical Pd_3Pt_1/C samples were selected for XPS analysis. It is known that the escape depth of photoelectrons for metals is ca. 20 Å. In our study, however, the obtained mean particle diameter for all the Pd_3Pt_1/C catalysts is around 5 nm (>20 Å). Therefore, Pd and Pt atoms on the surface layers of the catalysts can be detected by XPS. Fig. 2 shows XPS spectra of the Pd_3Pt_1/C-1 and Pd_3Pt_1/C-3 catalysts in the binding energy ranges of Pd_{3d} and Pt_{4f}. In Fig. 2a, each curve exhibits two Pd peaks, assigned to $Pd_{5/2}$ and $Pd_{3/2}$. The observed binding energies are close to those of metallic Pd, with binding energies of 335.2 and 340.4 eV, for $Pd_{5/2}$ and $Pd_{3/2}$, respectively [13,33,34], and much lower than those for palladium oxide that has corresponding binding energies of 338.1 and 343.0 eV [35,36], indicating that Pd in the Pd_3Pt_1/C samples exists mostly in its metallic state. The binding energies for these two Pd_3Pt_1/C catalysts are shifted to higher energies with respect to the corresponding peaks of metallic Pd, which could be ascribed to the mutual interaction between Pd and Pt, as well as the formation of Pd/Pt alloys. Furthermore, the binding energies for the Pd_3Pt_1/C-1 are slightly lower than those for the Pd_3Pt_1/C-3, suggesting that the microenvironment and electronic properties for these two catalysts are different.

In Fig. 2b, each curve shows two peaks located at ca. 71.2 and 74.8 eV, which are assigned to the Pt $4f_{7/2}$ and Pt $4f_{5/2}$ levels of metallic platinum, respectively, [37,38]. The binding energies for the two Pd_3Pt_1/C samples are slightly shifted to lower binding energy compared to the corresponding peaks of metallic Pt. Again, such a shift can be attributable to the interaction between the Pd and Pt, as supported by Pd XPS studies.

According to the peak area ratio of $Pd_{3d}$and Pt_{4f}, as determined from the peaks shown in Fig. 2a and b, the Pd/Pt surface atomic ratios of the Pd_3Pt_1/C-1 and Pd_3Pt_1/C-3 catalysts are estimated to be 1.54 and 4.36, respectively, clearly indicating Pt enrichment on the surface layers of Pd_3Pt_1/C-1 catalyst and Pd enrichment on the surface layers of Pd_3Pt_1/C-3 catalyst when compared with the Pd/Pt bulk composition of 3:1. The underlying mechanism of surface Pt enrichment of the Pd_3Pt_1/C-1 catalyst might be attributed to the fact that the decomposition temperature of $Pd(acac)_2$ is much lower than that of $Pt(acac)_2$, thus leading to more Pt atoms on the surface layers of the catalyst. Alternatively, the Pd_3Pt_1/C-3 catalyst with Pd enrichment on the surface layers might be attributed to the formation of complexes of TC with Pd and Pt after the addition of TC during the synthesis. Similar conclusions can be drawn for the Pd_3Pt_1/C-2 and Pd_3Pt_1/C-4 catalysts.

In order to get more insight into surface microstructures of the catalysts, CO-stripping voltammograms of the commercial Pt/C, Pd/C and two Pd_3Pt_1/C catalysts are shown in Fig. 3. From the figure, it is clear that the oxidation peaks of adsorbed CO species on the Pd_3Pt_1/C catalysts are located at the intermediate position between Pt/C and Pd/C catalysts. Note that the $(CO)_{ad}$ oxidation peak on the Pd_3Pt_1/C-1 catalyst is closer to that on the Pt/C catalyst; however, the $(CO)_{ad}$ oxidation peak on the Pd_3Pt_1/C-3 catalyst, which is shifted to more positive potential compared with that on the Pd_3Pt_1/C-1 catalyst, is closer to that on the Pd/C catalyst. The results clearly indicate that the Pt enrichment on the surface layers was formed on the Pd_3Pt_1/C-1 catalyst and the Pd enrichment on the surface layers was formed on the Pd_3Pt_1/C-3 catalyst, which are in qualitative agreement with the data obtained from XPS. Furthermore, the CO tolerance increases in the order of Pt/C < Pd_3Pt_1/C-1 < Pd_3Pt_1/C-3 < Pd/C, probably due to the effect of surface Pd/Pt composition of the catalysts – implying that the methanol tolerance of the catalysts may increase in the same order. It is worth mentioning that adsorbed CO oxidation involves only a single peak on the Pd_3Pt_1/C catalysts, suggesting that the peak is not simply an addition of fractional contributions of Pt and Pd sites and that a synergistic effect is evident [39]. Thus, from XPS and CO-stripping voltammetric results, one can conclude that the surface Pd/Pt composition can be tuned by adding TC as complexing agent during the synthesis.

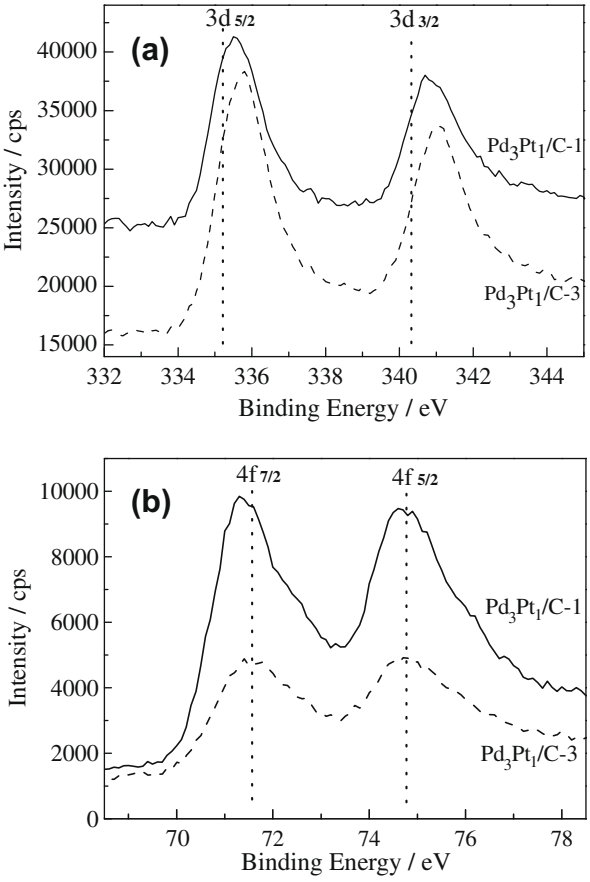

Fig. 2. XPS spectra of the Pd_3Pt_1/C-1 and Pd_3Pt_1/C-3 catalysts in the binding energy ranges of (a) Pd 3d, and (b) Pt 4f.

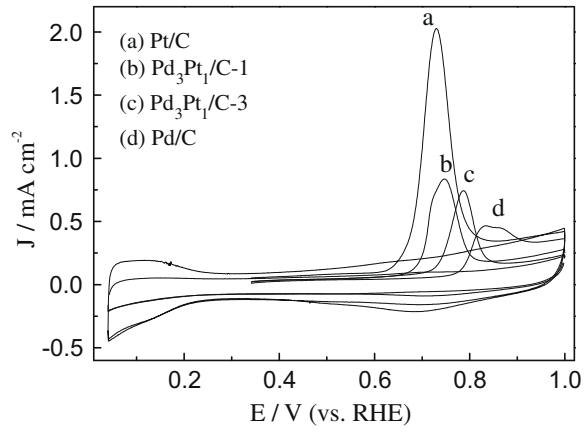

Fig. 3. CO-stripping voltammograms of the Pt/C, Pd/C, and two Pd_3Pt_1/C catalysts in 0.1 M $HClO_4$ at a scan rate of 20 mV s^{-1}. Current densities are normalized to the geometric surface area.

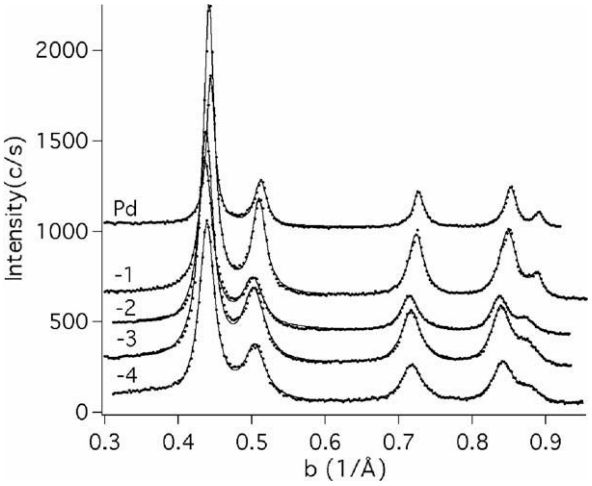

Fig. 4. The corrected diffraction patterns of the Pd/C and Pd_3Pt_1/C catalysts versus $b = 2\sin\theta/\lambda$. Solid lines are Lorentzian profile fits.

3.2. Structural studies

High quality X-ray diffraction data combined with an accurate line profile fitting have been acquired. The WAXS patterns of the as-prepared carbon-supported Pd_3Pt_1 bimetallic catalysts and the Pd/C catalyst background contribution, corrected for angular factors of polarization, absorption, and geometric effects, are provided in Fig. 4. The resultant patterns are fitted with Lorentzian functions, which closely resemble the experimental profiles, plus a residual linear background, and can provide a wealth of information of the nanoparticles defect structure. As shown in Fig. 4, all of the patterns can be fitted using a continuous functional form for the five observable Bragg peaks (111), (200), (220), (311), and (222), demonstrating that all the as-prepared bimetallic catalysts contain the single-phase disordered Pd or Pt fcc-structure (i.e., solid solution).

The integrated line widths δb of 5 peak fits exhibit fluctuations as shown in Fig. 5a, which can be attributed to size broadening ($\delta b_L = 1/L$), where L is the mean crystallite size, and additional *hkl*-dependent broadening contributions [40] that may have different origins:

(i) Stacking faults, $\delta b_\alpha = (1.5\alpha + \beta)K_{hkl}$, caused by the departure from the ideal fcc stacking sequences ABCABC..., which may be deformation faults (probability α) and/or twinning faults (probability β). K_{hkl} in this expression is a factor between 0.43 and 1 depending on the indices *hkl* [41];
(ii) Internal lattice strains $\delta b_\sigma = 2b\sigma/E_{hkl}$, where σ is the RMS intrinsic strain, E_{hkl} is the Young's modulus [41]; and
(iii) Fluctuation δc in the composition of individual particles about the average composition c_0 of the alloy system: $\delta b_c = \delta c(b/a)(da/dc)$, where da/dc is the change in the lattice constant (a) with compositional change.

There is a distinct variation in the width from peak to peak, which would not be expected for pure size broadening. Simple size broadening would produce a straight horizontal line in this graph, independent of the individual Bragg peaks. The patterns are similar for the samples Pd_3Pt_1-2, -3, and -4. But there is a slight systematic shift of the high-order Bragg peaks 220 and 311.[1] Sample Pd_3Pt_1/C-1 was subjected to a hydration/dehydration cycle prior to a peak

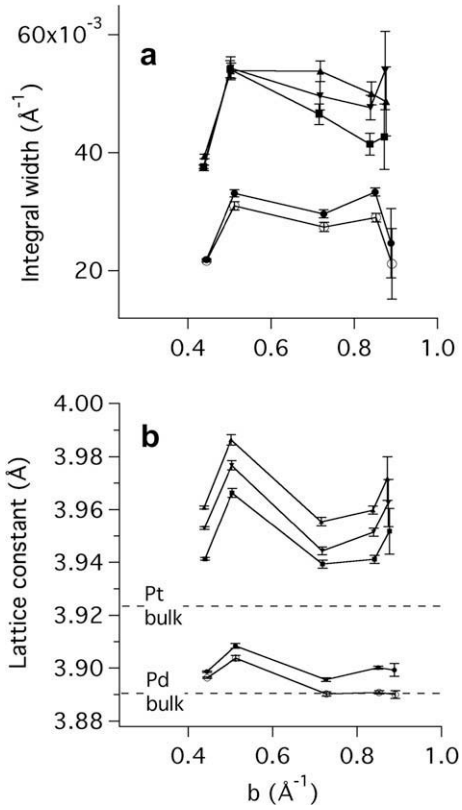

Fig. 5. (a) Integrated line widths, and (b) lattice constants determined from five reflections: (111), (200), (220), (311), and (222). The samples are labeled as follows: Pd: ∓; Pd_3Pt_1/C-1: ℓ; Pd_3Pt_1/C-2: ←; Pd_3Pt_1/C-3: ↔; Pd_3Pt_1/C-4: ◆. Line shifts of the individual peaks are affected by deformation stacking faults.

fitting routine to form a more homogenous alloy system by exposure to H_2 at room temperature and successive heating to 170 °C.[2] Together with the pure Pd/C catalyst, these line widths differ distinctly from those of the samples Pd_3Pt_1/C-2, -3, and -4 prepared by the addition of TC.

Since the four parameters L, $(1.5\alpha + \beta)$, σ, and δc affect each other, they can be only roughly determined from the measured integrated line width. Their proximal numbers are provided in Table 1.

Samples Pd_3Pt_1/C-2, -3, and -4 are similar, with high stacking defect probability between 6% and 9%, and compositional fluctuations between 2% and 3%. The differences are seen as a slight increase of stacking faults with the amount of TC added during the synthesis. Samples Pd_3Pt_1/C-1 and Pd/C have less stacking faults and no compositional fluctuations. The crystallite size is larger, with L between 7 and 8 nm, and internal strains go up to ~103 N/mm^2. At present, the origin of such a large strain is unclear.

Warren's theory predicts a characteristic line shift induced by deformation stacking faults [41], following the equation: $b_{hkl} = a/(h^2 + k^2 + l^2)^{1/2}$, where $a = a_0(1 - \alpha A_{hkl})$, with A_{hkl} being a constant, $-0.07 < A_{hkl} < +0.03$ [42]. Since the b_{hkl}-values are determined with high accuracy, the variations in a can be clearly observed (cf. Fig. 5b). Again, these numbers can be fitted using a_0 and α as free parameters. The values a_0 are listed in Table 1. The numbers obtained for α agree with those of column 3 of Table 1, with the assumption that twinning probability is not significant ($\beta \approx 0$). Note that the lattice constants of samples Pd_3Pt_1/C-2, -3, -4 are

[1] The 222-peak width is very inaccurate, and has been excluded from the evaluations.

[2] In the *as-received* state of this sample, the line profiles are asymmetric, which makes the data evaluation inconsistent.

Table 1
X-ray data obtained from line profile analysis.

Sample	Lattice constant a_0 (Å)	Stacking fault prob. $1.5\alpha + \beta$ (%)	Internal strains b (N/mm^2)	Compositional fluctuations δb_c (%)	Mean crystallite size L (nm)
Pd/C	3.891	3.1 (2.1)[a]	700	0	7.1
Pd_3Pt_1/C-1[b]	3.899	2.3 (1.5)	1000	0	7.9
Pd_3Pt_1/C-2	3.960	6.1 (4.1)	<500	2	5.0
Pd_3Pt_1/C-3	3.949	8.7 (5.8)	<500	3	5.0
Pd_3Pt_1/C-4	3.943	8.9 (5.9)	<500	3	5.0

[a] Numbers in parentheses are the α-values for $\beta \approx 0$.
[b] Sample hydrated and dehydrated at 170 °C.

well above that of bulk platinum (a = 3.9236 Å), which is unexpected and unusual for alloy particles formed of Pd and Pt. The slight increase of a_0 from samples Pd_3Pt_1/C-2, -3 and -4 is correlated to the increase in the amount of TC during the synthesis. The observed lattice expansion for samples Pd_3Pt_1/C-2, -3, -4 is likely due to the stacking faults.

3.3. Hydration/dehydration studies

The study of hydrogen adsorption to palladium in its nanosized form has attracted much attention due to palladium's importance as a catalyst in hydration processes [43–45]. Only a few studies have focused on structural aspects of hydrogen dissolved in the volume of the particles [43,46,47]. In a prior publication, we have calculated the effect of the size mismatch for a core-shell cluster morphology [47]. It was found that the lattice constants extracted from the Debye function of the model cluster depend mainly on the interatomic distance of atom species that forms the cluster core. Accordingly, it is expected that hydride formation of clusters with a palladium core would produce a strong lattice expansion. On the other hand, a Pt core surrounded by Pd would not produce a strong lattice expansion. For the Pd-Pt binary system under investigation, X-ray diffraction should therefore be able to probe the degree of alloying, and/or to test for the formation of an intrinsic core-shell structure. In this study, hydration/dehydration experiments were performed with an in situ cell attached to the Guinier diffractometer [47,48]. Fig. 6 shows the diffraction patterns of three catalysts before (solid line, under vacuum) and after hydration (dashed line, at 1 bar of H_2) at room temperature.

Fig. 6 clearly shows a lattice expansion for sample Pd_3Pt_1/C-1, and the pure Pd/C catalyst after hydration. However, no expansion or only marginal expansion is observed for sample Pd_3Pt_1/C-3. This is in full agreement with the XPS and CO-stripping voltammetric results, which suggest a Pt-rich core for samples Pd_3Pt_1/C-2, -3, and -4, and a Pd-rich core for sample Pd_3Pt_1/C-1. For the as-prepared Pd_3Pt_1/C-1, the lattice constant is ca. 3.900 Å, which follows Vegard's law [48]. After hydration, the lattice constant expands to 3.995 Å, which is much larger than that of bulk platinum. However, after dehydration, the lattice constant goes down again to ca. 3.899 Å, which is the same as that of the as-prepared sample. The asymmetry of the line profile seen for sample Pd_3Pt_1/C-1 must be related to a certain degree of compositional inhomogeneity of this sample. The differences become more evident at the high-order Bragg peaks, as shown in Fig. 7. Thus, from WAXS studies, one can conclude that the core of sample Pd_3Pt_1/C-1 is enriched in Pd, while the core of samples Pd_3Pt_1/C-2, −3, and −4 is rich in Pt, since platinum is known not to dissolve hydrogen into its lattice. Such a conclusion is supported by XPS and CO stripping results.

3.4. Effects of the surface and structure of Pd_3Pt_1/C catalysts on the ORR activity in pure acidic and methanol-containing solution

As reported in the literature [7,49], Pt monolayer deposited on suitable metal substrates might enhance ORR activity significantly

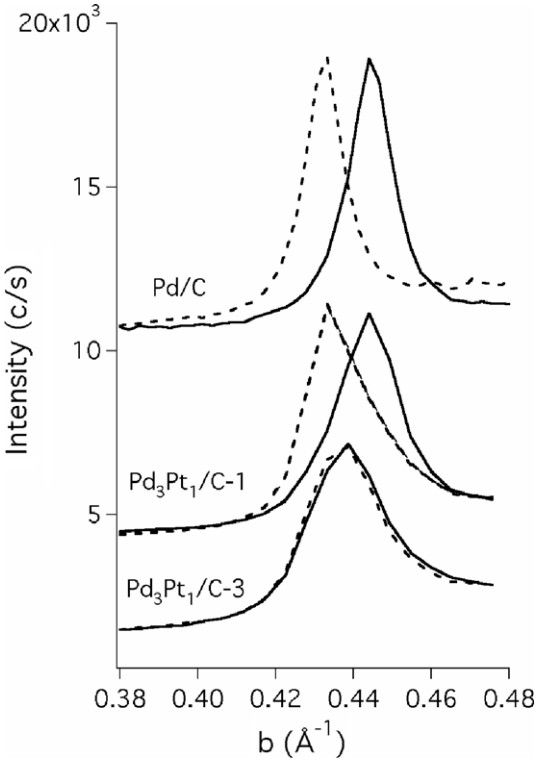

Fig. 6. Effect of hydride formation on the (111)-peak profile before (solid line, under vacuum), and after H_2 exposure (dashed line, at 1 bar H_2 at room temperature).

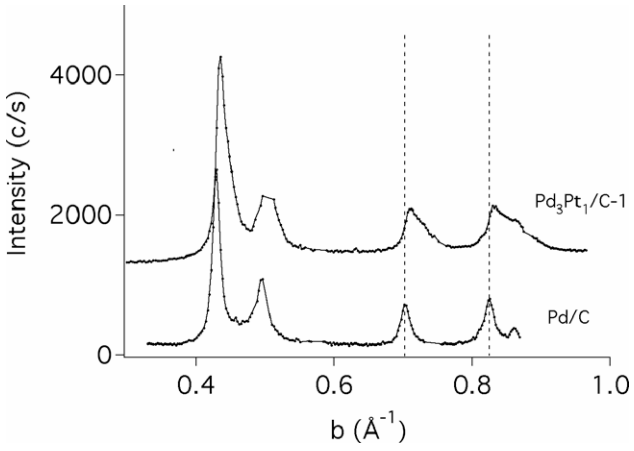

Fig. 7. Comparison of the full in situ diffraction patterns in the hydrated state of Pd/C and Pd_3Pt_1/C-1 catalysts.

with very low Pt loading, and the Pt_1Pd_1/C catalyst with a Pt skin layer shows slightly higher ORR activity than Pd_3Pt_1/C catalyst. Fig. 8 depicts the ORR on the commercial Pt/C and Pd_3Pt_1/C catalysts under the same experimental conditions. From the figure, the ORR on all the catalysts is shown to be diffusion controlled when the potential is less than 0.70 V, and under mixed control in the potential region between 0.70 and 0.85 V. When the potential is greater than 0.85 V, the ORR is found to be under kinetics control in the Tafel region. As can be seen, the ORR activity decreases in the order Pd_3Pt_1/C-1 > Pt/C > Pd_3Pt_1/C-3 > Pd_3Pt_1/C-2 > Pd_3Pt_1/C-4. The Pd_3Pt_1/C-1 catalyst with a Pt surface enrichment shows the highest ORR activity, and the activity for the ORR is slightly higher than that of the commercial Pt/C catalyst. However, commercial Pt/C catalyst shows a better ORR performance than the other three Pd_3Pt_1/C catalysts with Pd surface enrichment.

RRDE data shown in Fig. 8 are also illustrative of the ORR pathway on the Pt/C and Pd_3Pt_1/C catalysts. The fraction of peroxide, $X_{H_2O_2}$, at a typical fuel cell operating potential of 0.75 V/RHE, was evaluated from disk current (I_D), ring current (I_R), and collection factor ($N = 0.20$) using the equations: $X_{H_2O_2} = 2I/N/(I_D+I_R/N)$ [17]. The fractions are lower than 0.1% for the Pt/C and Pd_3Pt_1/C catalysts. Thus, the ORR reveals a negligible peroxide production on the Pd_3Pt_1/C catalysts and indicates a four-electron process leading to water formation.

Fig. 9 shows an ORR comparison on the commercial Pt/C and Pd_3Pt_1/C catalysts in the presence of 0.5 M CH_3OH. Compared to the ORR in pure acidic solution, all the catalysts show an increase in overpotential in the presence of methanol. The significant increase in overpotential (ca. 200 mV) of ORR on the Pt/C catalyst is due to the competition reaction between oxygen reduction and methanol oxidation; the overall process is a combination of the ORR and methanol oxidation reaction, which leads to the formation of the mixed potential. However, the potential losses of the ORR at 0.5 mA cm^{-2} on the Pd_3Pt_1/C-1, -2, -3, and -4 are ca. 35, 16, 15, and 13 mV, respectively. Obviously, the Pd_3Pt_1/C-3 catalyst shows the highest ORR activity, which is attributed to Pd enrichment on the surface layers, and the ORR activity in the kinetic and mixed regions on all the Pd_3Pt_1/C catalysts is much higher than that on the Pt/C catalyst, indicating that the Pd_3Pt_1/C catalysts exhibit a high methanol tolerance during the ORR.

To further understand the origin of high methanol tolerance of the Pd_3Pt_1/C catalysts during the ORR, the methanol oxidation reaction was studied in N_2-saturated solution under similar experimental conditions. Fig. 10 shows linear scanning voltammograms of the methanol oxidation on the Pt/C and Pd_3Pt_1/C catalysts in 0.5 M CH_3OH. The current densities of methanol oxidation on the Pd_3Pt_1/C catalysts are much lower than that of the Pt/C catalyst, and the methanol oxidation peak current densities decrease in the order Pt/C > Pd_3Pt_1/C-1 > Pd_3Pt_1/C-2 > Pd_3Pt_1/C-3 > Pd_3Pt_1/C-4. It is clear that the methanol tolerance of the Pd_3Pt_1/C catalysts increases with the amount of TC added into the reacting mixture. Thus, high methanol tolerance of the Pd_3Pt_1/C catalysts during the ORR is due to the weak competitive reaction of methanol oxidation, which could be induced by the composition effect associated with the presence of Pd atoms. The high tolerance of the Pd_3Pt_1/C catalysts to methanol suggests that the Pd_3Pt_1/C catalysts may be an economically viable candidate to replace Pt as a cathode catalyst in a DMFC.

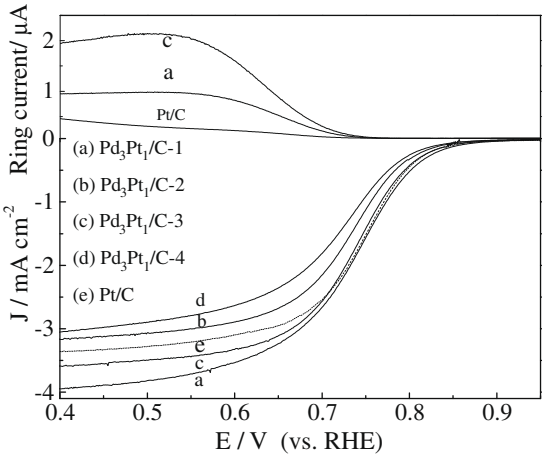

Fig. 8. Linear scan voltammograms (LSVs) of the Pt/C and Pd_3Pt_1/C catalysts in 0.1 M $HClO_4$ saturated with pure O_2 (5 mV s^{-1} and 1600 rpm). Current densities are normalized to the geometric surface area. The ring current, RRDE data, for the hydrogen peroxide production are contrasted.

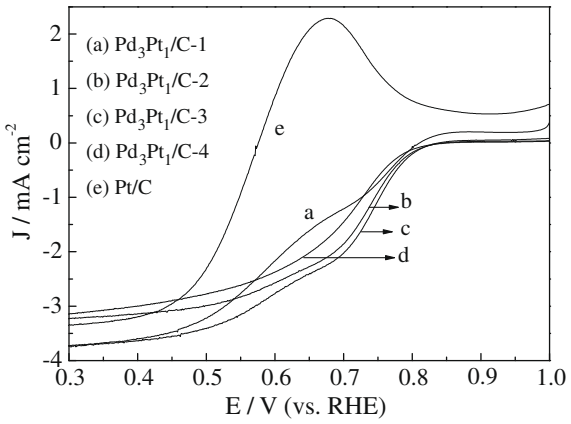

Fig. 9. LSVs of the Pt/C and Pd_3Pt_1/C catalysts in 0.1 M $HClO_4$ + 0.5 M CH_3OH saturated with pure O_2. The other conditions are identical to those shown in Fig. 8.

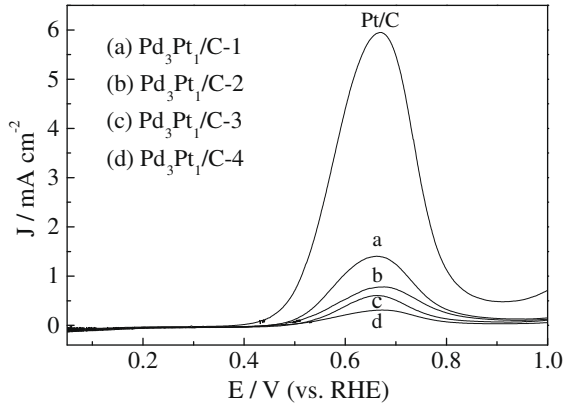

Fig. 10. LSVs of methanol oxidation on the Pt/C and Pd_3Pt_1/C catalysts in 0.1 M $HClO_4$ + 0.5 M CH_3OH saturated with pure N_2. The other conditions are identical to those shown in Fig. 8.

4. Conclusions

In summary, we reported a surface and structure-controlled synthesis of the Pd_3Pt_1/C catalysts for the ORR. XPS, CO-stripping voltammetric and WAXS results confirm that the addition of TC as the complexing agent during the synthesis leads to the formation of a Pd enrichment on the surface layers of the Pd_3Pt_1/C catalysts and to lattice expansion. Without the addition of TC, however, a normal lattice parameter and Pt enrichment on the surface layers of the catalysts are found. Furthermore, the Pd_3Pt_1/C catalysts prepared with the addition of TC have high stacking fault probability

(between 6% and 9%) and compositional fluctuations (between 2% and 3%). For the Pd/C catalyst and the Pd_3Pt_1/C catalysts prepared without the addition of TC, however, there are fewer stacking faults and no compositional fluctuations. Interestingly, the highest ORR activity was observed for the Pd_3Pt_1/C catalyst that exhibited Pt surface enrichment; and the activity, in fact, surpasses that of state-of-the-art Pt/C catalyst. However, the Pd_3Pt_1/C catalysts with the Pd surface enrichment exhibit much higher methanol tolerance during the ORR. Thus, since Pd is more abundant and much cheaper than Pt, Pd_3Pt_1/C catalysts may represent a promising type of catalyst for selective ORR in a DMFC.

Acknowledgments

We would like to thank the NSF of China (20673136), the National "863" Programs of China (2006AA05Z136, 2007AA05Z141, 2008AA05Z102), and the 100 People Plan Program of the Chinese Academy of Sciences for support of this work.

References

[1] E. Reddington, A. Sapienza, B. Gurau, R. Viswanathan, S. Sarangapani, E.S. Somtkin, T.E. Mallouk, Science 280 (1998) 1735.
[2] C. Roychowdhury, F. Matsumoto, V.B. Zeldovich, S.C. Warren, P.F. Mutolo, M. Ballesteros, U. Wiesner, H.D. Abruna, F.J. Disalvo, Chem. Mater. 18 (2006) 3365.
[3] S. Song, Y. Wang, P. Tsiakaras, P.K. Shen, Appl. Catal. B 78 (2008) 381.
[4] J.A. Kerres, J. Membr. Sci. 185 (2001) 3.
[5] Y. Fu, A. Manthiram, M.D. Guiver, Electrochem. Commun. 9 (2007) 905.
[6] H. Yang, W. Vogel, C. Lamy, N. Alonso-Vante, J. Phys. Chem. B 108 (2004) 11024.
[7] J. Zhang, Y. Mo, M.B. Vukmirovic, R. Klie, K. Sasaki, R.R. Adzic, J. Phys. Chem. B 108 (2004) 10955.
[8] E. Antolini, T. Lopes, E.R. Gonazlez, J. Alloys Compd. 461 (2008) 253.
[9] O. Savadogo, K. Lee, K. Oishi, S. Mitsushima, N. Kamiya, K.I. Ota, Electrochem. Commun. 6 (2004) 105.
[10] J.L. Fernandez, D.A. Walsh, A.J. Bard, J. Am. Chem. Soc. 127 (2005) 357.
[11] V. Raghuveer, A. Manthiran, A.J. Bard, J. Phys. Chem. B 109 (2005) 22909.
[12] J.L. Fernandez, V. Raghuveer, A. Manthiram, A.J. Bard, J. Am. Chem. Soc. 127 (2005) 13101.
[13] K. Lee, O. Savadogo, A. Ishihara, S. Mitsushima, N. Kamiya, K.I. Ota, J. Electrochem. Soc. 153 (2006) A20.
[14] W.E. Mustain, K. Kepler, J. Prakash, Electrochem. Commun. 8 (2006) 406.
[15] M.R. Tarasevich, G.V. Zhutaeva, V.A. Bogdanovskaya, M.V. Radina, M.R. Ehrenburg, A.E. Chalykh, Electrochim. Acta 52 (2007) 5108.
[16] M.H. Shao, K. Sasaki, R.R. Adzic, J. Am. Chem. Soc. 128 (2006) 3526.
[17] W. Wang, D. Zheng, C. Du, Z. Zou, X. Zhang, B. Xia, H. Yang, D.L. Akins, J. Power Sources 167 (2007) 243.
[18] M.H. Shao, P. Liu, J. Zhang, R. Adzic, J. Phys. Chem. B 111 (2007) 6772.
[19] L. Zhang, K. Lee, J. Zhang, Electrochim. Acta 52 (2007) 3088.
[20] Y. Suo, L. Zhang, J. Lu, Angew. Chem. Int. Ed. 46 (2007) 1.
[21] L. Zhang, K. Lee, J. Zhang, Electrochim. Acta 52 (2007) 7946.
[22] S. Tominaka, T. Momma, T. Osaka, Electrochim. Acta 53 (2008) 4679.
[23] T. Toda, H. Igarashi, H. Uchida, M. Watanabe, J. Electrochem. Soc. 146 (1999) 3750.
[24] K.T. Kim, Y.G. Kim, J.S. Chung, J. Electrochem. Soc. 142 (1995) 1531.
[25] K.T. Kim, J.T. Hwang, Y.G. Kim, J.S. Chung, J. Electrochem. Soc. 140 (1993) 31.
[26] H. Li, Q. Xin, W. Li, Z. Zhou, L. Jiang, S. Yang, G. Sun, Chem. Commun. (2004) 2776.
[27] W. Wang, Q. Huang, J. Liu, Z. Zou, Z. Li, H. Yang, Electrochem. Commun. 10 (2008) 1396.
[28] J. Yang, J.Y. Lee, Q. Zhang, W. Zhou, Z. Liu, J. Electrochem. Soc. 155 (2008) B776.
[29] K.D. Beard, J.W.V.J. Zee, R. Monnier, Appl. Catal. B: Environ. 0 (2008) 0, doi:10.1016/j.apcatb.2008.09.33.
[30] H. Li, G. Sun, N. Li, S. Sun, D. Su, Q. Xin, J. Phys. Chem. C 111 (2007) 5605.
[31] S. Liao, K.A. Holmes, H. Tsaprailis, V.I. Birss, J. Am. Chem. Soc. 128 (2006) 3504.
[32] R. Wang, S. Liao, Z. Fu, Electrochem. Commun. 10 (2008) 523.
[33] T. Thurn-Albrecht, J. Schotter, G.A. Kästle, N. Emley, T. Shibauchi, L. Krusin-Elbaum, K. Guarini, C.T. Black, M.T. Tuominen, T.P. Russell, Science 290 (2000) 2126.
[34] C.W. Yi, K. Luo, T. Wei, D.W. Goodman, J. Phys. Chem. B 109 (2005) 18535.
[35] J.F. Moulder, W.F. Stickle, P.E. Sobol, K.D. Bomben, Handbook of X-ray photoelectron spectroscopy, in: J. Chastain (Ed.), Perkin-Elmer Corporation Physical Electronics Division, Eden Prairie, MN, 1992.
[36] H. Meng, S.H. Sun, J.P. Masse, J.P. Dodelet, Chem. Mater. 20 (2008) 6998.
[37] A.S. Arico, A.K. Shukla, H. Kim, S. Park, M. Min, V. Antonucci, Appl. Surf. Sci. 33 (2001) 172.
[38] J.J. Huang, H. Yang, Q.H. Huang, Y.W. Tang, T.H. Lu, D.L. Akins, J. Electrochem. Soc. 151 (2004) A1810.
[39] A.C. Garcia, V. Paganin, E.A. Ticianelli, Electrochim. Acta 53 (2008) 4309.
[40] W. Vogel, B. Tesche, W. Schulze, Chem. Phys. 74 (1983) 137.
[41] B.E. Warren, X-ray Diffraction, Addison-wesley, Reading, 1969.
[42] C.N.J. Wagner, A.S. Tetelman, H.M. Otte, J. Appl. Phys. 33 (1962) 3080.
[43] H. Kobayashi, M. Yamauchi, H. Kitagawa, Y. Kubota, K. Kato, M. Takata, J. Am. Chem. Soc. 130 (2008) 1828.
[44] C. Sachs, A. Pundt, R. Kirchheim, M. Winter, M.T. Reetz, D. Fritsch, Phys. Rev. B 64 (2001) 75408.
[45] D. Teschner, Z. Revay, J. Borsodi, M. Haevecker, A. Knop-Gericke, R. Schloegl, D. Milroy, D. Torres, P. Sautet, Angew. Chem. Int. Ed. 47 (2008) 1.
[46] A. Pundt, D.M. Ornheim, M. Guerdane, H. Teichler, H. Ehrenberg, M.T. Reetz, N.M. Jisrawi, Eur. Phys. J. D19 (2002) 333.
[47] W. Vogel, P. Britz, H. Bonnemann, J. Rothe, J. Hormes, J. Phys. Chem. B 101 (1997) 11029.
[48] H. Boennemann, W. Brijoux, R.A. Brinkmann, S. Tilling, T. Schilling, B. Tesche, K. Seevogel, R. Franke, J. Hormes, G. Kohl, J. Pollmann, J. Rothe, W. Vogel, Inorg. Chim. Acta 270 (1998) 95.
[49] J. Zhang, M.B. Vukmirovic, K. Sasaki, A.U. Nilekar, M. Mavrikakis, R.R. Adzic, J. Am. Chem. Soc. 127 (2005) 12480.